 https://doi.org/10.3311/PPci.41126

Periodica Polytechnica Civil Engineering, 69(4), pp. 1244–1262, 2025

Closed-form Solutions for Lateral Displacement of Single-bay Coupled Shear Walls Using a Subsystem-based Three-field CTB Beam

Mao Cristian Pinto-Cruz[1,2*]

[1] Department of Civil and Environmental Engineering, Pontifical Catholic University of Rio de Janeiro, Rua Marquês de São Vicente 225., 22451-900 Rio de Janeiro, Brazil
[2] Department of Civil Engineering, National University of Engineering, Avenue Túpac Amaru 210., 15333 Lima, Peru
[*] Corresponding author, e-mail: mao.pinto.c@uni.pe

Received: 26 May 2025, Accepted: 08 September 2025, Published online: 10 October 2025

Abstract

Local shear deformation and axial extensibility of walls have recently been recognized as critical, yet previously overlooked, sources of error in predicting the lateral displacement of coupled shear walls. Existing analytical models often face limited practical application due to solution complexity and insufficient physical clarity. Using a generalized continuous model, this paper proposes a simple, exact, closed-form analytical formulation based on an independent subsystem approach, enabling fast and accurate estimation of lateral displacements. The generalized continuous model couples, in parallel, an extensible Timoshenko beam and a shear beam, thereby capturing both shear deformation and axial extensibility. The total lateral displacement is expressed as a linear combination of three independent subsystems: bending, shear, and bending–shear coupling. Closed-form solutions are derived for each subsystem under uniform, triangular, and top-concentrated loading. The displacement components—bending, shear, and interaction—are physically interpreted, with the interaction term arising exclusively from the coupling subsystem. Numerical examples illustrate the physical meaning of each component, while a parametric analysis establishes applicability limits, showing a maximum safe-side error of +7.30%, compared to the −56.04% unsafe-side error of the classical solution. The proposed formulation ensures structural safety, maintains analytical simplicity, and is well-suited for practical engineering design.

Keywords

coupled shear wall, three-field CTB beam, lateral displacement, local shear deformation, axial extensibility, analytical solutions, exact solutions

1 Introduction

Coupled shear walls (hereafter, CSWs) are highly efficient lateral-load-resisting systems that provide stability under wind and seismic actions. Their performance—governed by stiffness, strength, and energy dissipation capacity—depends strongly on the height and mechanical properties of the coupling beams, which improve overall behavior compared with uncoupled wall systems. Although advanced finite element method (SAP2000 software [1]) allows detailed numerical modeling and is widely accessible to structural engineers, closed-form analytical solutions remain valuable. These solutions offer minimal computational cost, ease of implementation (often enabling rapid hand calculations), and are effective for verifying numerical models, particularly in large datasets. They also facilitate targeted evaluation of key load-resisting mechanisms and promote intuitive understanding of structural behavior. Among the analytical approaches, the continuous method is widely applied to approximate the global response of CSW. This method idealizes the discrete wall–beam configuration as an equivalent continuous beam by uniformly distributed the stiffness of the beams along the height, thereby capturing layered wall–beam interaction and representing the shear walls as cantilever elements under lateral loading.

The continuous method is commonly traced to the work of Letitia Chitty, who first investigated the static behavior of parallel interconnected beams [2] and subsequently proposed a parallel-coupled continuous model—comprising a bending beam and a shear beam—for the analysis of tall buildings [3], though without accounting for

Cite this article as: Pinto-Cruz, M. C. "Closed-form Solutions for Lateral Displacement of Single-bay Coupled Shear Walls Using a Subsystem-based Three-field CTB Beam", Periodica Polytechnica Civil Engineering, 69(4), pp. 1244–1262, 2025. https://doi.org/10.3311/PPci.41126

axial extensibility of the vertical elements. This pioneering framework led to widespread adoption and further development of analytical and numerical strategies for tall buildings. Finite element models [4–6] and transfer matrix methods [7, 8] have been employed to investigate the static, dynamic, and stability behavior of sandwich beams, enabling representation of coupled shear walls, wall–frame interactions, and hybrid systems through equivalent continuous beam formulations. Simplified analytical solutions have also been proposed for routine engineering applications, including refinements incorporating axial extensibility [9] and semi-analytical formulations for global buckling analysis [10, 11]. Energy-based approaches have yielded equivalent stiffness equations for sandwich beams representing entire structural systems, capturing complex subsystem interactions [12, 13]. Closed-form expressions have been introduced for lateral displacement, natural frequency, and global buckling load estimation in both symmetric and asymmetric configurations [14–17]. More recent work has extended the method to CSWs with cavities [18], generalized drift estimation [19], CSWs with stiffening beams [20], coupling ratio evaluation [21], and studies linking dynamic response to stability performance [22].

Although substantial progress has been achieved in the development of analytical and numerical models for assessing static, dynamic, and stability behavior, classical formulations have systematically neglected two critical deformation mechanisms: local shear deformation and axial extensibility of walls. This omission has led to significant discrepancies in accuracy analyses, resulting in a sense of uncertainty among structural engineers and thereby severely limiting their practical application.

A recently developed generalized continuous beam formulation, referred to as the three-field CTB beam, integrates both local shear and bending deformation mechanisms through the parallel coupling of an extensible Timoshenko beam and a shear-type beam. Initially proposed by Capuani et al. [23] via an energy-based approach for the numerical analysis of coupled shear walls under static loading, the model was later extended to incorporate local shear effects associated with bending and torsional deformations in non-uniform structural cores with open or closed thin-walled sections [24]. Subsequent advancements included applications to soil–structure interaction and the dynamic response of wall–frame systems [25, 26]. Capsoni and Moghadasi Faridani [27] further refined the model by formulating numerical solutions for both static and dynamic analyses and by integrating energy dissipation devices into single-bay coupled shear wall systems [28, 29]. More recently, generalized analytical and numerical solutions have been introduced for static, dynamic, and stability analyses [30–32].

Despite their generality and rigorous theoretical foundations, the practical implementation of these models often requires advanced technical expertise, entails complex procedures, and provides limited insight into the separate contributions of bending, shear, and their interactions. Furthermore, their applicability is constrained by the absence of publicly available implementation tools and by their limited suitability for routine engineering workflows.

To overcome these limitations, this study employs the three-field CTB beam, with five primary objectives:

1. to integrate local shear deformation and axial extensibility of the walls into the classical sandwich beam formulation;
2. to decompose the total lateral displacement as the linear combination of three independent subsystems;
3. to derive closed-form analytical expressions for rapid and accurate estimation of lateral displacement;
4. to decompose the total lateral displacement into three distinct components of structural relevance—bending, shear, and bending–shear interaction; and
5. to introduce a static correction factor that accounts for the additional deformation mechanism, thereby enhancing the predictive accuracy of existing analytical models.

The paper is structured into six main sections. Section 2 introduces the generalized continuous beam and its equivalent stiffnesses. Section 3 details the decomposition approach into independent subsystems. Section 4 presents newly derived closed-form expressions for lateral displacement together with a proposed static correction factor. Section 5 validates the analytical formulations through numerical simulations and an extensive parametric study. Finally, Section 6 summarizes the principal findings and discusses potential avenues for future research.

2 Description of the generalized continuous model

The generalized continuum model results from the parallel coupling of an extensible Timoshenko beam and a shear beam (Fig. 1), referred to in the literature as the Three-field CTB Beam and hereafter denoted as the GCTB beam. This continuous model captures four types of deformation mechanisms—global bending, global shear, local

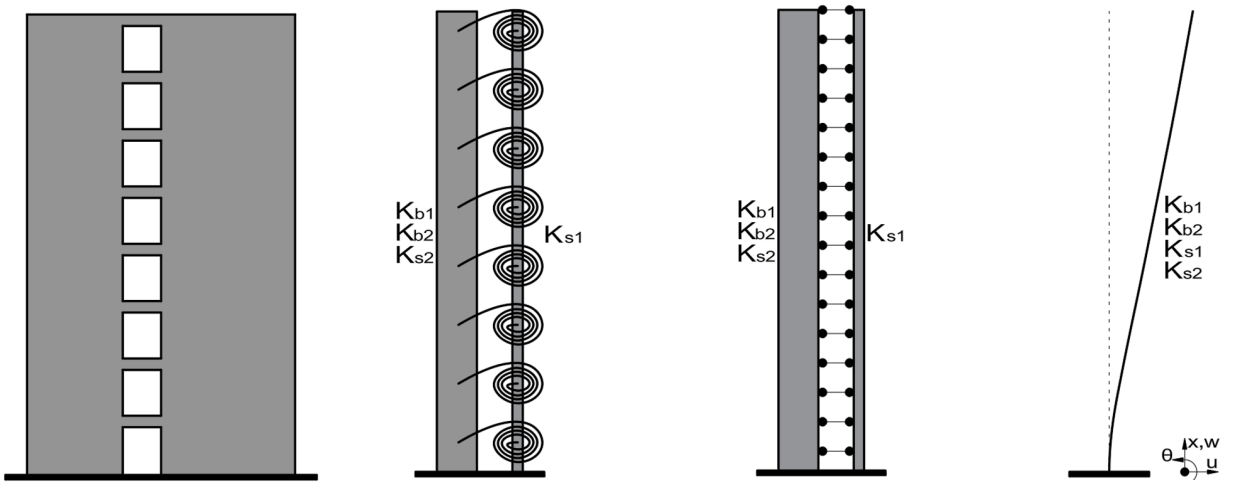

Fig. 1 Idealization process of a discrete coupled shear wall into an equivalent continuous model: (a) coupled shear wall; (b) parallel coupling of an extensible Timoshenko beam and a shear beam; (c) inextensible rigid links; and (d) equivalent continuous column

bending, and local shear—by varying the orders of magnitude of its equivalent stiffnesses. The model is fixed at the base (Fig. 1), and the mechanism association (Fig. 2) illustrates how its four equivalent stiffnesses are coupled. The extensible Timoshenko beam includes, in series, the global bending stiffness (K_{b1}), local bending stiffness (K_{b2}), and and local shear stiffness (K_{s2}), while the shear beam contributes the global shear stiffness (K_{s1}). The continuous model features three kinematic fields: lateral displacement (u), rotational displacement (θ), and axial displacement (w).

The equivalent stiffnesses are calculated as [30–32]:

$$K_{b1} = EA_2\left(1+\frac{A_2}{A_1}\right) \tag{1}$$

$$K_{s1} = G_{eq}t_b l_b \tag{2}$$

$$K_{b2} = E\left(I_1 + I_2\right) \tag{3}$$

$$K_{s2} = Gr\left(A_1 + A_2\right) \tag{4}$$

where

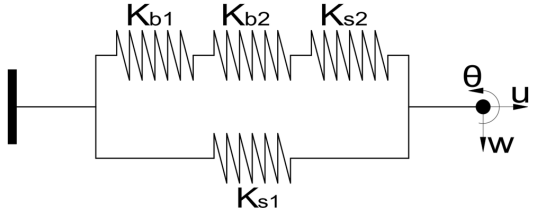

Fig. 2 Schematic representation of mechanisms arranged in series and in parallel

$$G_{eq} = \frac{1}{t_b h}\left(\frac{l_b'^2}{12EI_b}+\frac{1}{rGA_b}\right)^{-1} \tag{5}$$

$$l_b' \approx l_b\left(1+0.5\frac{h_b}{l_b}\right) \tag{6}$$

where E, G, I_1, I_2, A_1, A_2, G_{eq}, t_b, h_b, l_b, A_b, I_b, h and r denote, respectively, the Young's modulus, the shear modulus, the second moment of area of the left wall, the second moment of area of the right wall, the cross-sectional area of the left wall, the cross-sectional area of the right wall, the shear modulus of the equivalent continuous core, the beam width, the beam height, the clear span between walls, the beam cross-sectional area, the beam second moment of area, the story height, and the shear correction factor of the beam.

Two dimensionless parameters, α and κ, are introduced to characterize the type of behavior—shear, interaction, or bending—and the influence of axial deformations, respectively:

$$\alpha = H\sqrt{\frac{K_{s1}K_{s2}}{K_{b2}\left(K_{s1}+K_{s2}\right)}} \tag{7}$$

$$\kappa = \sqrt{\left(m+1\right)^2 + n^2\frac{K_{b2}}{K_{b1}}} \tag{8}$$

where

$$m = \frac{B_1 + B_2}{2l_b} \tag{9}$$

$$n = \frac{1 + A_2 / A_1}{l_b} \tag{10}$$

H is the total height of the continuous model.

The GCTB beam and its proposed analytical solutions are based on six key assumptions:

1. the material behavior is linear elastic, and the small displacement hypothesis is applicable;
2. the discrete shear forces in the coupling beams are replaced by an equivalent continuous shear flow;
3. the shear walls are subjected to plane stress conditions and possess rigid cross-sections;
4. the coupling beams are assumed to be axially inextensible;
5. the rotational fields of the walls are considered identical; and
6. both the coupling beams and the shear walls are modeled as Timoshenko beams, wherein strain energy arises from both bending and shear deformations.

Although the continuous model imposes no formal restriction on the number of stories, maintaining the validity of the homogenization hypothesis and ensuring acceptable accuracy in lateral displacement predictions requires a minimum of five stories. While this modeling framework has previously been applied to the analysis of coupled shear walls with non-uniform properties, the present study focuses exclusively on uniform configurations, wherein the equivalent stiffness parameters remain constant along the height of the structure.

3 Decomposition into independent subsystems

The sixth-order differential equation was recently established in the literature [30, 31], and is here expressed in normalized form using the dimensionless variable $z = x/H$:

$$u_{\mathrm{GCTB}}^{(6)}(z) - \frac{K_{s1}K_{s2}\left((m+1)^2 K_{b1} + n^2 K_{b2}\right)}{K_{b1}K_{b2}\left(K_{s1}+K_{s2}\right)} H^2 u_{\mathrm{GCTB}}^{(4)}(z) = -\frac{1}{K_{s1}+K_{s2}} H^2 f^{(4)}(z) + \frac{K_{b1}\left(m^2 K_{s1} + K_{s2}\right) + n^2 K_{s1}K_{b2}}{K_{b1}K_{b2}\left(K_{s1}+K_{s2}\right)} H^4 f''(z) - \frac{n^2 K_{s1}K_{s2}}{K_{b1}K_{b2}\left(K_{s1}+K_{s2}\right)} H^6 f(z) \tag{11}$$

where $f(z)$ is the lateral load distributed along the continuous model.

Notably, the differential equation governing the classical sandwich beam (hereinafter, SWB beam) can be recovered as a special case of the GCTB beam formulation by assuming that the local shear stiffness tends to infinity ($K_{s2} \to \infty$) and by setting $m = 0$ and $n = 1$; that is,

$$u^{(6)}(z) - \frac{K_{s1}\left(K_{b1}+K_{b2}\right)}{K_{b1}K_{b2}} H^2 u^{(4)}(z) = \frac{H^4}{K_{b2}}\left[f''(z) - \frac{K_{s1}}{K_{b1}K_{b2}} H^2 f(z) \right]. \tag{12}$$

By starting from the governing differential equation of the classical sandwich beam (SWB beam) and examining the relative magnitudes of global and local bending and shear stiffnesses, it becomes possible to systematically derive the differential equations corresponding to other classical continuous beam models. For example:

- Euler-Bernoulli beam (hereafter, EBB beam):

$$u_{\mathrm{EBB}}^{(4)}(z) = \frac{H^4}{K_{b2}} f(z) \tag{13}$$

- Shear beam (hereafter, SB beam):

$$u_{\mathrm{SB}}''(z) = -\frac{H^2}{K_{s1}} f(z) \tag{14}$$

- Parallel coupling of the bending beam and the shear beam (hereafter, CTB beam):

$$u_{\mathrm{CTB}}^{(6)}(z) - \frac{K_{s1}}{K_{b2}} H^2 u_{\mathrm{CTB}}^{(4)}(z) = \frac{H^4}{K_{b2}} f''(z). \tag{15}$$

To decompose the lateral displacement, the total lateral displacement $u(z)$ is expressed as the superposition of three independent displacement components, $u_1(z)$, $u_2(z)$, and $u_3(z)$, such that:

$$u_{\mathrm{GCTB}}(z) = u_1(z) + u_2(z) + u_3(z). \tag{16}$$

By substituting Eq. (16) into Eq. (11) and performing straightforward algebraic manipulations, the following expression is obtained:

$$\left[u_1^{(6)}(z)+u_2^{(6)}(z)-\frac{K_{s1}K_{s2}\left((m+1)^2K_{b1}+n^2K_{b2}\right)}{K_{b1}K_{b2}\left(K_{s1}+K_{s2}\right)}H^2u_1^{(4)}(z)-\frac{K_{s1}K_{s2}\left((m+1)^2K_{b1}+n^2K_{b2}\right)}{K_{b1}K_{b2}\left(K_{s1}+K_{s2}\right)}H^2u_3^{(4)}(z)\right.$$
$$\left.-\frac{K_{b1}\left(m^2K_{s1}+K_{s2}\right)+n^2K_{s1}K_{b2}}{K_{b1}K_{b2}\left(K_{s1}+K_{s2}\right)}H^4f''(z)\right] \tag{17}$$
$$+\left[-\frac{K_{s1}K_{s2}\left((m+1)^2K_{b1}+n^2K_{b2}\right)}{K_{b1}K_{b2}\left(K_{s1}+K_{s2}\right)}H^2u_2^{(4)}(z)+\frac{n^2K_{s1}K_{s2}}{K_{b1}K_{b2}\left(K_{s1}+K_{s2}\right)}H^6f(z)\right]+\left[u_3^{(6)}(z)+\frac{1}{K_{s1}+K_{s2}}H^2f^{(4)}(z)\right]=0.$$

In this way, three subsystems can be distinguished:

- Subsystem 1
  The first subsystem is derived from the second bracket term.

$$u_2^{(4)}(z)=\left[1-(m+1)^2\frac{1}{\kappa^2}\right]\frac{H^4}{K_{b2}}f(z) \tag{18}$$

  or

$$u_2^{(4)}(z)=\left(\frac{1}{p_1^2}\right)\frac{H^4}{K_{b2}}f(z) \tag{19}$$

  where

$$p_1=\frac{1}{\sqrt{1-(m+1)^2\frac{1}{\kappa^2}}}. \tag{20}$$

  The resulting differential equation corresponds to the bending beam, where the static response is multiplied by the factor $\left(\frac{1}{p_1^2}\right)$.

- Subsystem 2
  The second subsystem is obtained from the third bracket. After four integrations and application of the corresponding boundary conditions, the resulting expression is:

$$u_3''(z)=-\left(\frac{1}{p_2^2}\right)\frac{H^2}{K_{s1}}f(z) \tag{21}$$

  where

$$p_2=\sqrt{1+\frac{K_{s2}}{K_{s1}}}. \tag{22}$$

  The resulting differential equation represents a shear beam, where the static response is scaled by a factor of $\left(\frac{1}{p_2^2}\right)$.

- Subsystem 3
  Once the first and second subsystems are obtained, Eqs. (19) and (21) are introduced into the first subsystem derived from the first bracket:

$$u_1^{(4)}(z)-\alpha^{*2}u_1''(z)=\left(\frac{1}{p_3^2}\right)\frac{H^4}{K_{b2}}f(z) \tag{23}$$

  where

$$p_3=\frac{1}{\sqrt{\frac{\left(\kappa^2-2m-1\right)K_{s1}^2-2mK_{s1}K_{s2}+K_{s2}^2}{\left(K_{s1}+K_{s2}\right)^2}-\left[1-(m+1)^2\frac{1}{\kappa^2}\right]}} \tag{24}$$

$$\alpha^*=\alpha\kappa. \tag{25}$$

  The resulting differential equation corresponds to the parallel coupling between the bending and shear beams, where the static response is multiplied by a factor of $\left(\frac{1}{p_3^2}\right)$.

Finally, the displacement of the GCTB beam is expressed as the linear combination of the independent displacements of the three subsystems:

$$u_{\mathrm{GCTB}}(z)=\left(\frac{1}{p_1^2}\right)u_{\mathrm{EBB}}(z)+\left(\frac{1}{p_2^2}\right)u_{\mathrm{SB}}(z)+\left(\frac{1}{p_3^2}\right)u_{\mathrm{CTB}}(z). \tag{26}$$

In this way, the complex static solution of the GCTB beam is decomposed as the linear combination of three independent subsystems: the EBB beam, the SB beam, and the CTB beam. For these subsystems, evaluating their static response is straightforward, since each is defined by a single degree of freedom associated with lateral displacement, and their governing differential equations have a lower order than the original problem. This decomposition not only facilitates the derivation of the analytical solution but also enables a clearer physical interpretation of the role of each deformation mechanism in the overall structural response. An important observation from this decomposition is that the displacement associated with the EBB beam and the SB beam are independent, which implies that the bending–shear interaction is fully contained within the CTB beam. It should be noted that this decomposition is also valid for the boundary conditions; therefore, in the static case, the decomposition is exact.

4 Analytical solutions

After establishing the decomposition of lateral displacement into independent subsystems—along with the corresponding governing differential equations and boundary conditions for each—this section presents closed-form analytical solutions, suitable for fast and accurate calculations, to estimate the lateral displacement of the GCTB beam under three classical lateral loading scenarios. Specifically, the following cases are considered:

1. a uniformly distributed lateral load (hereafter, uniform load),
2. a linearly varying lateral load (hereafter, triangular load), and
3. a concentrated lateral load applied at the top of the structure (hereafter, concentrated load).

These loading configurations are schematically illustrated in Fig. 3.

4.1 Particular case: uniformly distributed load $f(z) = w$

The static displacements of the three subsystems are expressed as follows:

- Subsystem 1

$$\left(\frac{1}{p_1^2}\right)u_{\mathrm{EBB}}(z)=\frac{wH^4}{\frac{(m+1)^2}{n^2}K_{b1}+K_{b2}}\left(\frac{1}{4}z^2-\frac{1}{6}z^3+\frac{1}{24}z^4\right) \tag{27}$$

- Subsystem 2

$$\left(\frac{1}{p_2^2}\right)u_{\mathrm{SB}}(z)=\frac{wH^2}{K_{s1}+K_{s2}}\left(z-\frac{1}{2}z^2\right) \tag{28}$$

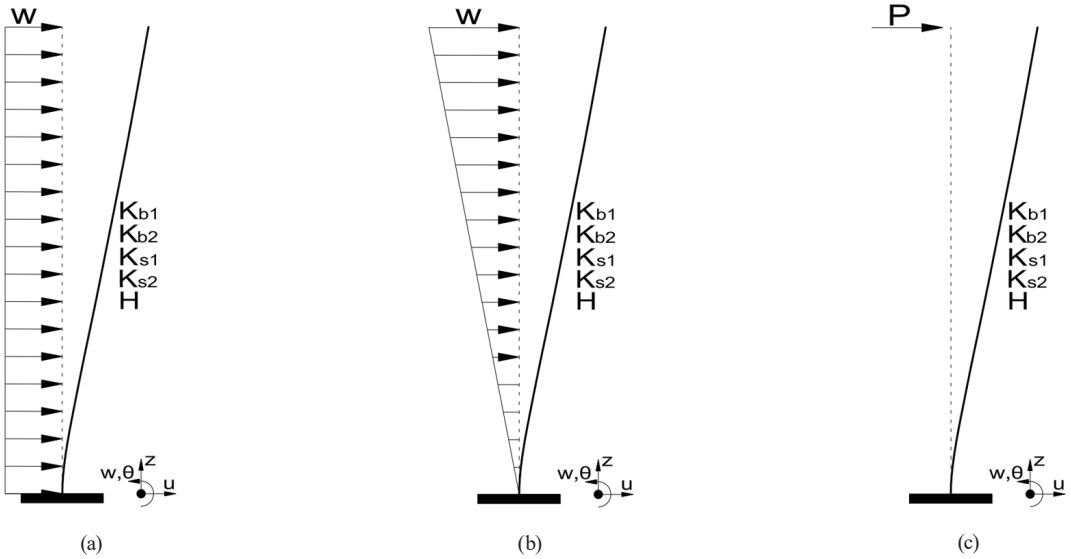

(a) (b) (c)

Fig. 3 Standard load cases: (a) Uniform load, (b) Triangular load, and (c) Concentrated load

- Subsystem 3

$$\left(\frac{1}{p_3^2}\right)u_{\mathrm{CTB}}(z)=\frac{1}{p_3^2(\alpha\kappa)^2}\frac{wH^4}{K_{b2}}\left(z-\frac{1}{2}z^2\right)-\frac{wH^4}{p_3^2(\alpha\kappa)^2K_{b2}}\left\{-\frac{\left[1+(\alpha\kappa)\sinh(\alpha\kappa)\right]\left[\cosh(\alpha\kappa z)-1\right]}{(\alpha\kappa)^2\cosh(\alpha\kappa)}+\frac{\sinh(\alpha\kappa z)}{(\alpha\kappa)}\right\}. \tag{29}$$

The displacement of the GCTB beam is expressed as the sum of the independent displacements of the three subsystems:

$$u_{\mathrm{GCTB}}(z)=\left(\frac{1}{p_1^2}\right)u_{\mathrm{EBB}}(z)+\left(\frac{1}{p_2^2}\right)u_{\mathrm{SB}}(z)+\left(\frac{1}{p_3^2}\right)u_{\mathrm{CTB}}(z) \tag{30}$$

i.e.,

$$u_{\mathrm{GCTB}}(z)=\frac{wH^4}{\frac{(m+1)^2}{n^2}K_{b1}+K_{b2}}\left(\frac{1}{4}z^2-\frac{1}{6}z^3+\frac{1}{24}z^4\right)+\frac{wH^2}{K_{s1}+K_{s2}}\eta\left(z-\frac{1}{2}z^2\right)$$
$$-\frac{wH^2}{K_{s1}+K_{s2}}(\eta-1)\left\{-\frac{\left[1+(\alpha\kappa)\sinh(\alpha\kappa)\right]\left[\cosh(\alpha\kappa z)-1\right]}{(\alpha\kappa)^2\cosh(\alpha\kappa)}+\frac{\sinh(\alpha\kappa z)}{(\alpha\kappa)}\right\} \tag{31}$$

where η is the proposed static correction factor to incorporate the local shear deformation mechanism of the walls into the classical formulation:

$$\eta=1+\frac{1}{(p_3\kappa)^2}\frac{(K_{s1}+K_{s2})^2}{K_{s1}K_{s2}}. \tag{32}$$

The total displacement $u(z)$ can be expressed as the sum of three displacement components: the bending component $u_f(z)$, the shear component $u_s(z)$, and the interaction component $u_i(z)$ between bending and shear:

$$u_{\mathrm{GCTB}}(z)=u_f(z)+u_s(z)+u_i(z) \tag{33}$$

where

$$u_f(z)=\frac{wH^4}{\frac{(m+1)^2}{n^2}K_{b1}+K_{b2}}\left(\frac{1}{4}z^2-\frac{1}{6}z^3+\frac{1}{24}z^4\right) \tag{34}$$

$$u_s(z)=\frac{wH^2}{K_{s1}+K_{s2}}\eta\left(z-\frac{1}{2}z^2\right) \tag{35}$$

$$u_i(z)=-\frac{wH^2}{K_{s1}+K_{s2}}(\eta-1)\left\{-\frac{\left[1+(\alpha\kappa)\sinh(\alpha\kappa)\right]\left[\cosh(\alpha\kappa z)-1\right]}{(\alpha\kappa)^2\cosh(\alpha\kappa)}+\frac{\sinh(\alpha\kappa z)}{(\alpha\kappa)}\right\}. \tag{36}$$

The static correction factor multiplies the displacement due to shear and interaction. Additionally, it is observed that the bending displacement has an equivalent stiffness of $\left[\frac{(m+1)^2}{n^2}K_{b1}+K_{b2}\right]$ where the global bending stiffness (K_{b1}) is amplified by a factor of $\frac{(m+1)^2}{n^2}$.

The maximum displacement is obtained at $z = 1$:

$$u_{\max}=\frac{wH^4}{8\left[\frac{(m+1)^2}{n^2}K_{b1}+K_{b2}\right]}+\frac{wH^2}{2(K_{s1}+K_{s2})}\eta-\frac{wH^2}{K_{s1}+K_{s2}}(\eta-1)\left[\frac{1+(\alpha\kappa)\sinh(\alpha\kappa)}{(\alpha\kappa)^2\cosh(\alpha\kappa)}-\frac{1}{(\alpha\kappa)^2}\right]. \tag{37}$$

4.2 Particular case: linearly distributed load $f(z) = wz$

The static displacements of the three subsystems are expressed as follows:

- Subsystem 1

$$\left(\frac{1}{p_1^2}\right)u_{\mathrm{EBB}}(z)=\frac{wH^4}{\frac{(m+1)^2}{n^2}K_{b1}+K_{b2}}\left(\frac{1}{6}z^2-\frac{1}{12}z^3+\frac{1}{120}z^5\right) \tag{38}$$

- Subsystem 2

$$\left(\frac{1}{p_2^2}\right)u_{\mathrm{SB}}(z)=\frac{wH^2}{K_{s1}+K_{s2}}\left(\frac{1}{2}z-\frac{1}{6}z^3\right) \tag{39}$$

- Subsystem 3

$$\left(\frac{1}{p_3^2}\right)u_{\mathrm{CTB}}(z)=\frac{1}{p_3^2(\alpha\kappa)^2}\frac{wH^4}{K_{b2}}\left(\frac{1}{2}z-\frac{1}{6}z^3\right)$$
$$-\frac{1}{p_3^2(\alpha\kappa)^2}\frac{wH^4}{K_{b2}}\left\{-\frac{\left[1+\frac{1}{2}\beta(\alpha\kappa)\sinh(\alpha\kappa)\right]\left[\cosh(\alpha\kappa z)-1\right]}{(\alpha\kappa)^2\cosh(\alpha\kappa)}+\frac{1}{2}\beta\frac{\sinh(\alpha\kappa z)}{(\alpha\kappa)}+\frac{1}{(\alpha\kappa)^2}z\right\} \tag{40}$$

where

$$\beta=1-\frac{2}{(\alpha\kappa)^2}. \tag{41}$$

The displacement of the GCTB beam is expressed as the sum of the independent displacements of the three subsystems:

$$u_{\mathrm{GCTB}}(z)=\frac{wH^4}{\frac{(m+1)^2}{n^2}K_{b1}+K_{b2}}\left(\frac{1}{6}z^2-\frac{1}{12}z^3+\frac{1}{120}z^5\right)+\frac{wH^2}{K_{s1}+K_{s2}}\eta\left(\frac{1}{2}z-\frac{1}{6}z^3\right)$$
$$-\frac{wH^2}{K_{s1}+K_{s2}}(\eta-1)\left\{-\frac{\left[1+\frac{1}{2}\beta(\alpha\kappa)\sinh(\alpha\kappa)\right]\left[\cosh(\alpha\kappa z)-1\right]}{(\alpha\kappa)^2\cosh(\alpha\kappa)}+\frac{1}{2}\beta\frac{\sinh(\alpha\kappa z)}{(\alpha\kappa)}+\frac{1}{(\alpha\kappa)^2}z\right\} \tag{43}$$

where η is the proposed static correction factor to incorporate the local shear deformation mechanism of the walls into the classical formulation:

$$\eta=1+\frac{1}{(p_3\kappa)^2}\frac{(K_{s1}+K_{s2})^2}{K_{s1}K_{s2}}. \tag{44}$$

The total displacement $u(z)$ can be expressed as the sum of three displacement components: the bending component $u_f(z)$, the shear component $u_s(z)$, and the interaction component $u_i(z)$ between bending and shear:

$$u_{\mathrm{GCTB}}(z)=\left(\frac{1}{p_1^2}\right)u_{\mathrm{EBB}}(z)+\left(\frac{1}{p_2^2}\right)u_{\mathrm{SB}}(z)+\left(\frac{1}{p_3^2}\right)u_{\mathrm{CTB}}(z) \tag{42}$$

i.e.,

$$u_{\mathrm{GCTB}}(z)=u_f(z)+u_s(z)+u_i(z) \tag{45}$$

where

$$u_f(z)=\frac{wH^4}{\frac{(m+1)^2}{n^2}K_{b1}+K_{b2}}\left(\frac{1}{6}z^2-\frac{1}{12}z^3+\frac{1}{120}z^5\right) \tag{46}$$

$$u_s(z)=\frac{wH^2}{K_{s1}+K_{s2}}\eta\left(\frac{1}{2}z-\frac{1}{6}z^3\right) \tag{47}$$

$$u_i(z) = -\frac{wH^2}{K_{s1}+K_{s2}}(\eta-1)\left\{-\frac{\left[1+\frac{1}{2}\beta(\alpha\kappa)\sinh(\alpha\kappa)\right]\left[\cosh(\alpha\kappa z)-1\right]}{(\alpha\kappa)^2\cosh(\alpha\kappa)}+\frac{1}{2}\beta\frac{\sinh(\alpha\kappa z)}{(\alpha\kappa)}+\frac{1}{(\alpha\kappa)^2}z\right\}. \tag{48}$$

The static correction factor multiplies the displacement due to shear and interaction. Additionally, it is observed that the bending displacement has an equivalent stiffness of $\left[\frac{(m+1)^2}{n^2}K_{b1}+K_{b2}\right]$ where the global bending stiffness (K_{b1}) is amplified by a factor of $\frac{(m+1)^2}{n^2}$.

The maximum displacement is obtained at $z = 1$:

$$u_{\max} = \frac{11wH^4}{120\left[\frac{(m+1)^2}{n^2}K_{b1}+K_{b2}\right]}+\frac{wH^2}{3(K_{s1}+K_{s2})}\eta-\frac{wH^2}{K_{s1}+K_{s2}}(\eta-1)\left[\frac{1+\frac{1}{2}\beta(\alpha\kappa)\sinh(\alpha\kappa)}{(\alpha\kappa)^2\cosh(\alpha\kappa)}\right]. \tag{49}$$

4.3 Particular case: concentrated load $P \neq 0$

The static displacements of the three subsystems are expressed as follows:

- Subsystem 1

$$\left(\frac{1}{p_1^2}\right)u_{\mathrm{EBB}}(z) = \frac{PH^3}{\frac{(m+1)^2}{n^2}K_{b1}+K_{b2}}\left(\frac{1}{2}z^2-\frac{1}{6}z^3\right) \tag{50}$$

- Subsystem 2

$$\left(\frac{1}{p_2^2}\right)u_{\mathrm{SB}}(z) = \frac{PH}{K_{s1}+K_{s2}}(z) \tag{51}$$

- Subsystem 3

$$\left(\frac{1}{p_3^2}\right)u_{\mathrm{CTB}}(z) = \frac{1}{p_3^2(\alpha\kappa)^2}\frac{PH^3}{K_{b2}}(z)-\frac{1}{p_3^2(\alpha\kappa)^2}\frac{PH^3}{K_{b2}}\left\{-\frac{\sinh(\alpha\kappa)\left[\cosh(\alpha\kappa z)-1\right]}{(\alpha\kappa)\cosh(\alpha\kappa)}+\frac{\sinh(\alpha\kappa z)}{(\alpha\kappa)}\right\}. \tag{52}$$

The displacement of the GCTB beam is expressed as the sum of the independent displacements of the three subsystems:

$$u_{\mathrm{GCTB}}(z) = \left(\frac{1}{p_1^2}\right)u_{\mathrm{EBB}}(z)+\left(\frac{1}{p_2^2}\right)u_{\mathrm{SB}}(z)+\left(\frac{1}{p_3^2}\right)u_{\mathrm{CTB}}(z) \tag{53}$$

i.e.,

$$u_{\mathrm{GCTB}}(z) = \frac{PH^3}{\frac{(m+1)^2}{n^2}K_{b1}+K_{b2}}\left(\frac{1}{2}z^2-\frac{1}{6}z^3\right)+\frac{PH}{K_{s1}+K_{s2}}\eta z-\frac{PH}{K_{s1}+K_{s2}}(\eta-1)\left\{-\frac{\sinh(\alpha\kappa)\left[\cosh(\alpha\kappa z)-1\right]}{(\alpha\kappa)\cosh(\alpha\kappa)}+\frac{\sinh(\alpha\kappa z)}{(\alpha\kappa)}\right\} \tag{54}$$

where η is the proposed static correction factor to incorporate the local shear deformation mechanism of the walls into the classical formulation:

$$\eta = 1+\frac{1}{(p_3\kappa)^2}\frac{(K_{s1}+K_{s2})^2}{K_{s1}K_{s2}}. \tag{55}$$

The total displacement $u(z)$ can be expressed as the sum of three displacement components: the bending component $u_f(z)$, the shear component $u_s(z)$, and the interaction component $u_i(z)$ between bending and shear:

$$u_{\mathrm{GCTB}}(z) = u_f(z) + u_s(z) + u_i(z) \tag{56}$$

where

$$u_f(z) = \frac{PH^3}{\frac{(m+1)^2}{n^2}K_{b1} + K_{b2}}\left(\frac{1}{2}z^2 - \frac{1}{6}z^3\right) \tag{57}$$

$$u_s(z) = \frac{PH}{K_{s1} + K_{s2}}\eta z \tag{58}$$

$$u_i(z) = -\frac{PH}{K_{s1} + K_{s2}}(\eta - 1)\left\{-\frac{\sinh(\alpha\kappa)\left[\cosh(\alpha\kappa z) - 1\right]}{(\alpha\kappa)\cosh(\alpha\kappa)} + \frac{\sinh(\alpha\kappa z)}{(\alpha\kappa)}\right\}. \tag{59}$$

The static correction factor multiplies the displacement due to shear and interaction. Additionally, it is observed that the bending displacement has an equivalent stiffness of $\left[\frac{(m+1)^2}{n^2}K_{b1} + K_{b2}\right]$ where the global bending stiffness (K_{b1}) is amplified by a factor of $\frac{(m+1)^2}{n^2}$.

The maximum displacement is obtained at $z = 1$:

$$u_{\max} = \frac{PH^3}{3\left[\frac{(m+1)^2}{n^2}K_{b1} + K_{b2}\right]} + \frac{PH}{K_{s1} + K_{s2}}\eta - \frac{PH}{K_{s1} + K_{s2}}(\eta - 1)\left[\frac{\sinh(\alpha\kappa)}{(\alpha\kappa)\cosh(\alpha\kappa)}\right]. \tag{60}$$

5 Accuracy and precision of the proposed solutions

The accuracy and precision of the proposed closed-form analytical expressions for predicting the lateral displacement of CSWs will be verified through comparisons with numerical results obtained from the finite element method (SAP2000 software [1]). To evaluate the applicability of the proposed formulations for both symmetric and asymmetric CSWs, three distinct cases were investigated, as illustrated in Fig. 4: Case 1 involves a symmetric CSW with $L = 5$ m ($L_2/L_1 = 1$), and cases 2 and 3 correspond to asymmetric CSWs with length ratios of $L_2/L_1 = 1.5$ and $L_2/L_1 = 2$, respectively.

The story height was set at $h = 3$ m, the coupling beam depth at $h_b = 1$ m, and the width of both walls and coupling beams at $t = 0.3$ m. The material properties considered include an elasticity modulus $E = 30$ GPa and a shear modulus $G = 12.5$ GPa. Since the classical formulation was extended to incorporate the local shear deformation mechanism of the walls, the CSW system was required to exhibit various types of behavior, including bending, shear, and interaction effects. Therefore, to represent this range of behavioral modes, the number of stories was varied from 5 to 30, corresponding to total heights between 15 and 90 meters.

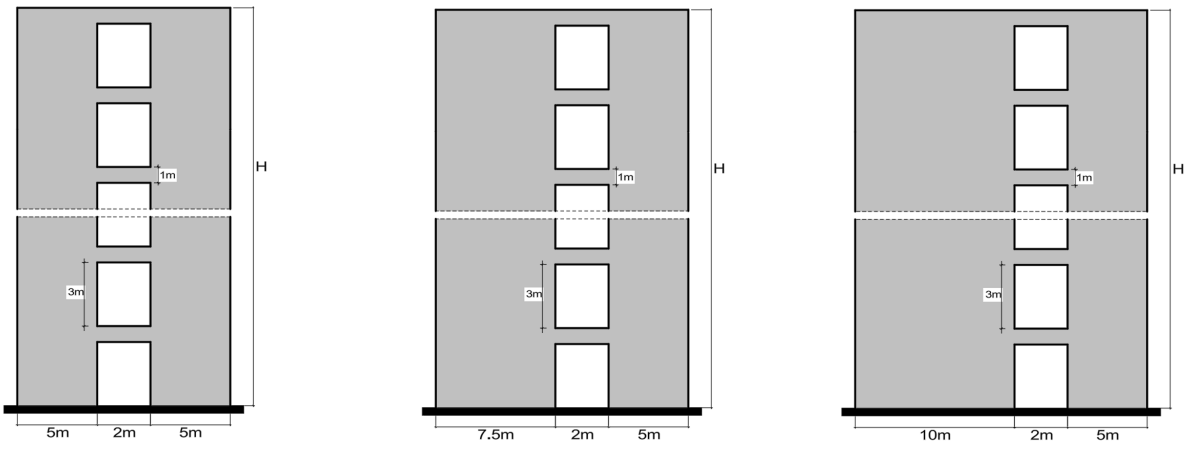

(a) (b) (c)

Fig. 4 Case studies: (a) Case 1 – symmetric CSW, $L_2/L_1 = 1$, (b) Case 2 – asymmetric CSW, $L_2/L_1 = 1.5$, and (c) Case 3 – asymmetric CSW, $L_2/L_1 = 2$

The stiffness of the walls and coupling beams was calculated based on the gross cross-sectional properties, neglecting concrete cracking and reinforcement contributions.

In the SAP2000 structural model, both the shear walls and coupling beams were represented using Timoshenko-type frame elements, incorporating both bending and shear deformations. The CSW was modeled using the equivalent frame approach, in which the walls and coupling beams were aligned along the centroidal axes of their respective cross-sections. To ensure appropriate force transfer and realistic connectivity between the structural components, rigid end offsets were introduced at beam–wall interfaces.

Three lateral load distributions were considered: a uniform load w = 20 kN/m, a triangular w = 20 kN/m, and a concentrated load P = 500 kN.

Figs. 5, 6, and 7 present the lateral displacement profiles of the CSW under uniform lateral loading (Case 1), as obtained from the proposed analytical solutions and compared with finite element method (FEM) results for 5-, 15-, and 30-story configurations, representing low-, mid-, and high-rise CSWs, respectively. The analytical predictions derived from the GCTB beam exhibit excellent agreement with FEM results across all CSW heights, including the low-rise case where local shear deformation plays a dominant role. In contrast, the SWB beam shows significant deviations, particularly in low-rise CSWs (Fig. 5), due to its omission of the local shear deformation mechanism, leading to inaccurate displacement estimates. These discrepancies diminish as CSW height increases (Figs. 6 and 7), becoming negligible for high-rise CSWs, where both GCTB and SWB beams provide comparable and accurate results—consistent with findings reported in the existing literature.

Figs. 5–7 also illustrate the individual displacement components—bending, shear, and bending–shear

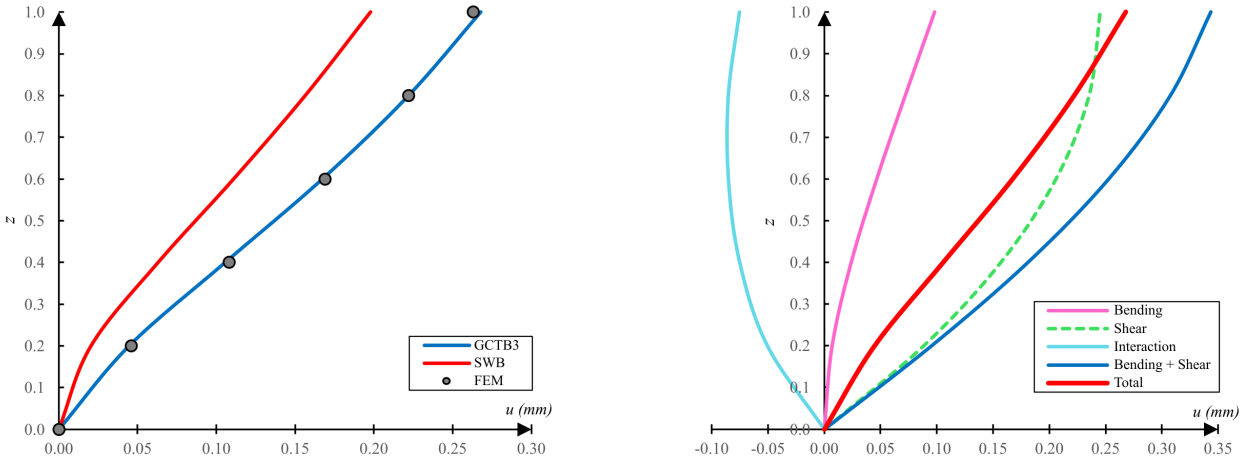

(a) (b)

Fig. 5 Case 1 – Lateral displacement of a 5-story CSW under uniform load: (a) Comparison of lateral displacements predicted by the GCTB and SWB beam; (b) Decomposition of GCTB beam displacement into bending, shear, and interaction components

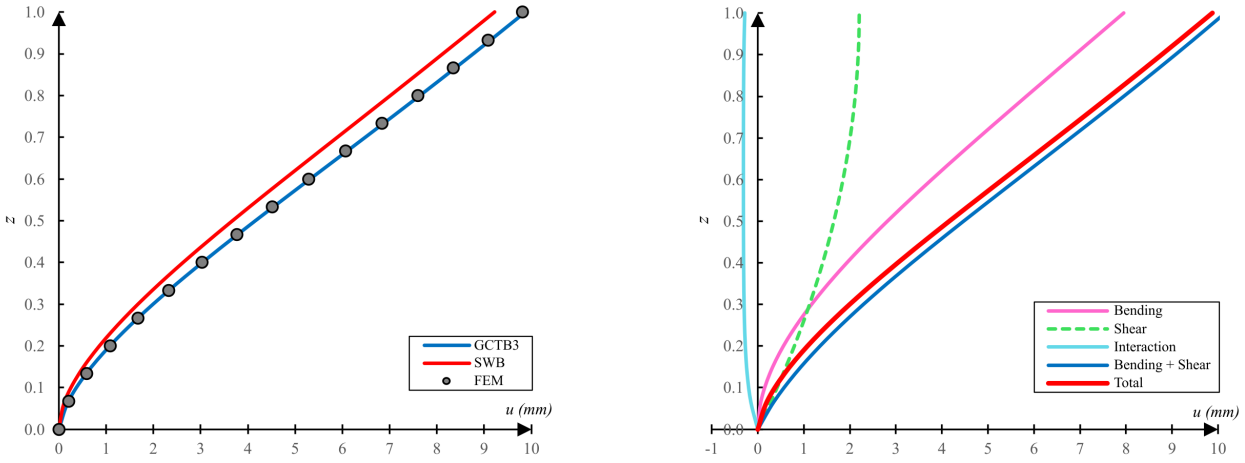

(a) (b)

Fig. 6 Case 1 – Lateral displacement of a 15-story CSW under uniform load: (a) Comparison of lateral displacements predicted by the GCTB and SWB beam; (b) Decomposition of GCTB beam displacement into bending, shear, and interaction components

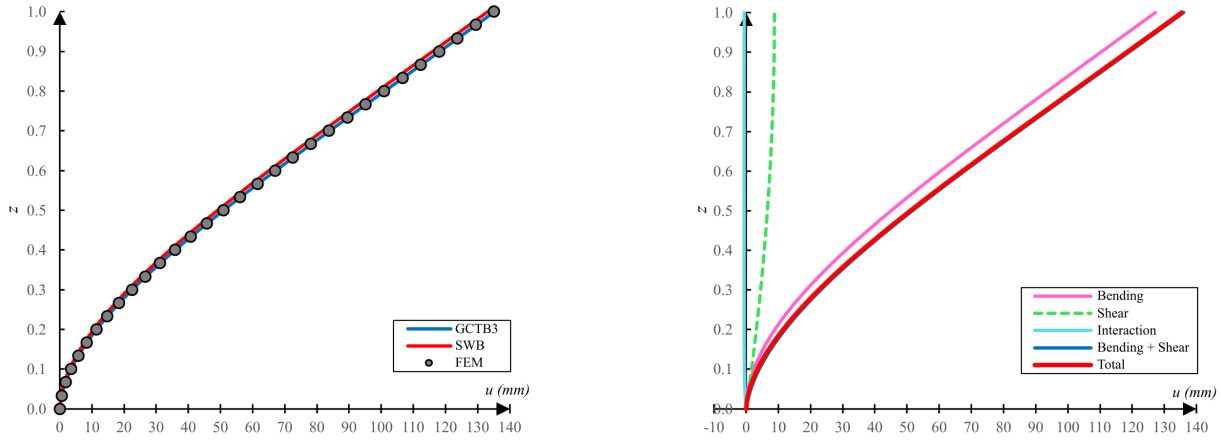

(a) (b)

Fig. 7 Case 1 – Lateral displacement of a 30-story CSW under uniform load: (a) Comparison of lateral displacements predicted by the GCTB and SWB beam; (b) Decomposition of GCTB beam displacement into bending, shear, and interaction components

interaction—as well as the combined response obtained by summing only the bending and shear components, excluding interaction. Several key observations can be made from these results:

- The interaction displacement decreases with CSW height and remains negative, thus reducing the total lateral displacement. While its omission simplifies estimation, this is only justifiable for mid- and high-rise CSWs, where the effect is negligible. In low-rise CSWs, however, the interaction contribution is substantial and must be included to ensure accuracy. Notably, this displacement component remains approximately uniform along the CSW height.
- The contribution of bending displacement increases with the height of the CSW, whereas the shear displacement decreases. Consequently, shear deformation predominates in low-rise CSWs, while flexure becomes the governing factor in medium- and high-rise CSWs.
- All three components—bending, shear, and interaction—are significant in low-rise CSWs, making their inclusion essential for accurate structural design. In mid-rise CSWs, the interaction component may be neglected without a significant loss of accuracy; however, both bending and shear must be considered. For high-rise CSWs, bending deformation alone is sufficient, as the contributions from shear and interaction become negligible.
- Mid-rise CSWs exhibit a transitional behavior characteristic of wall–frame systems, where bending is predominant in the lower stories and shear becomes more influential in the upper stories.

Figs. 8–10 extend this analysis to the asymmetric CSW with $L_2/L_1 = 1.50$ (Case 2), and Figs. 11–13 to the asymmetric CSW with $L_2/L_1 = 2$ (Case 3), under uniform loading. The conclusions drawn for the symmetric cases equally apply to these asymmetric configurations. However, the

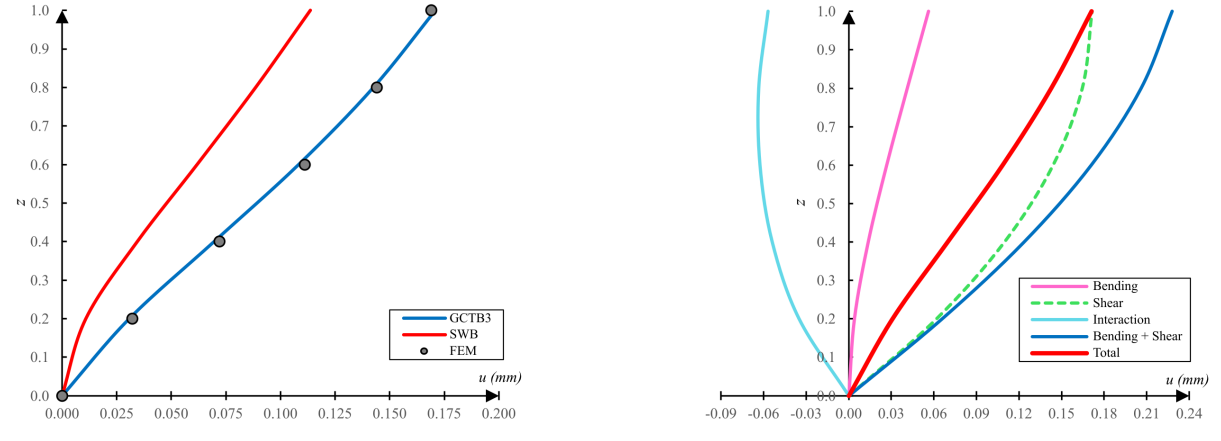

(a) (b)

Fig. 8 Case 2 – Lateral displacement of a 5-story CSW under uniform load: (a) Comparison of lateral displacements predicted by the GCTB and SWB beam; (b) Decomposition of GCTB beam displacement into bending, shear, and interaction components

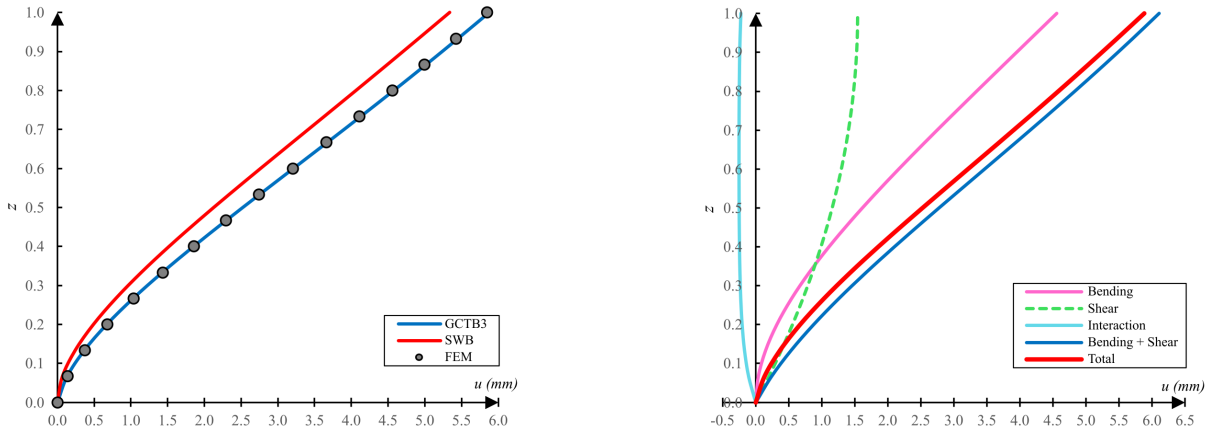

(a) (b)

Fig. 9 Case 2 – Lateral displacement of a 15-story CSW under uniform load: (a) Comparison of lateral displacements predicted by the GCTB and SWB beam; (b) Decomposition of GCTB beam displacement into bending, shear, and interaction components

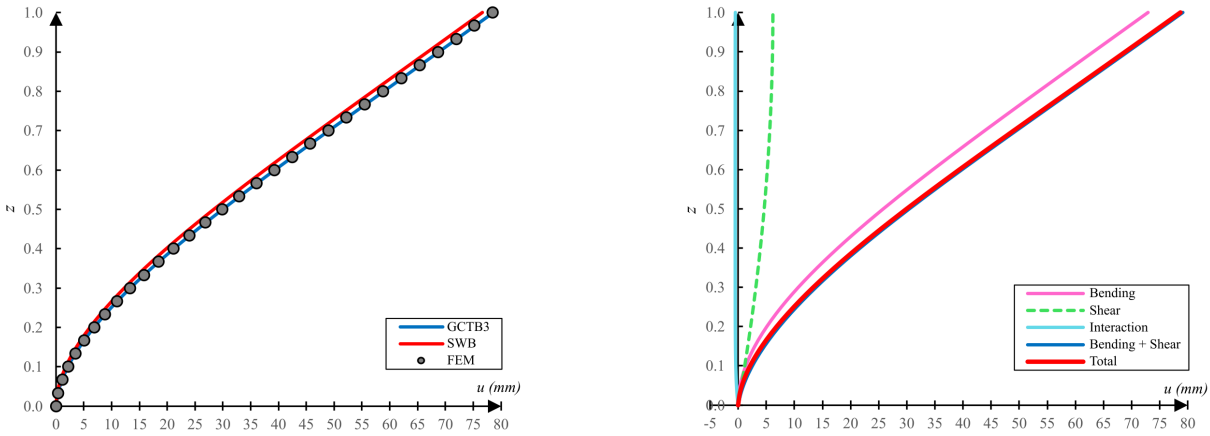

(a) (b)

Fig. 10 Case 2 – Lateral displacement of a 30-story CSW under uniform load: (a) Comparison of lateral displacements predicted by the GCTB and SWB beam; (b) Decomposition of GCTB beam displacement into bending, shear, and interaction components

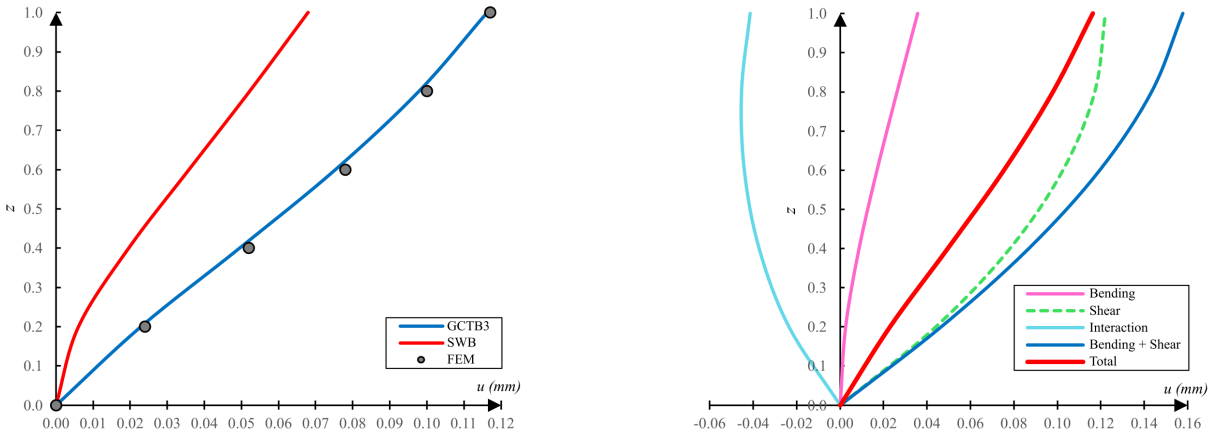

(a) (b)

Fig. 11 Case 3 – Lateral displacement of a 5-story CSW under uniform load: (a) Comparison of lateral displacements predicted by the GCTB and SWB beam; (b) Decomposition of GCTB beam displacement into bending, shear, and interaction components

local shear deformation mechanism exacerbates the errors of the SWB beam in low-rise asymmetric CSWs, with error magnitudes of approximately −24.76%, −32.75%, and −41.87% for Cases 1, 2, and 3, respectively, indicating

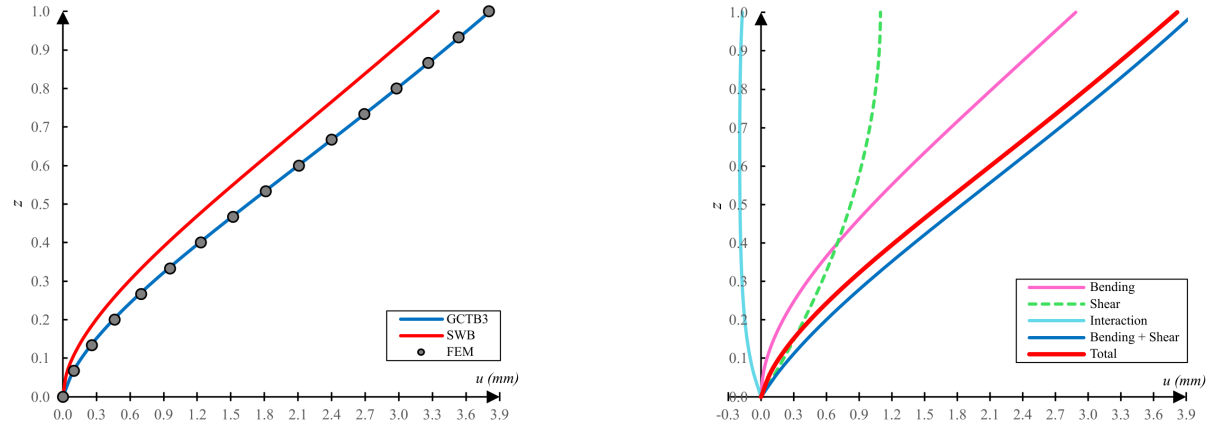

(a) (b)

Fig. 12 Case 3 – Lateral displacement of a 15-story CSW under uniform load: (a) Comparison of lateral displacements predicted by the GCTB and SWB beam; (b) Decomposition of GCTB beam displacement into bending, shear, and interaction components

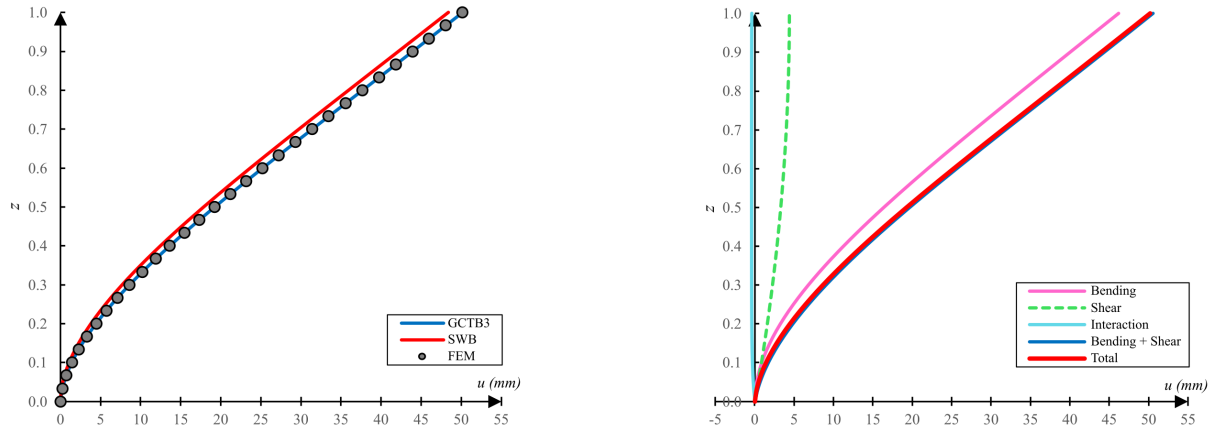

(a) (b)

Fig. 13 Case 3 – Lateral displacement of a 30-story CSW under uniform load: (a) Comparison of lateral displacements predicted by the GCTB and SWB beam; (b) Decomposition of GCTB beam displacement into bending, shear, and interaction components

that asymmetry introduces an additional error factor of about 1.7. These errors become negligible in medium- and high-rise asymmetric CSWs.

The lateral displacement solutions were also validated under triangular loading for low-rise CSWs (Figs. 14–16). Displacement profiles for bending and shear closely

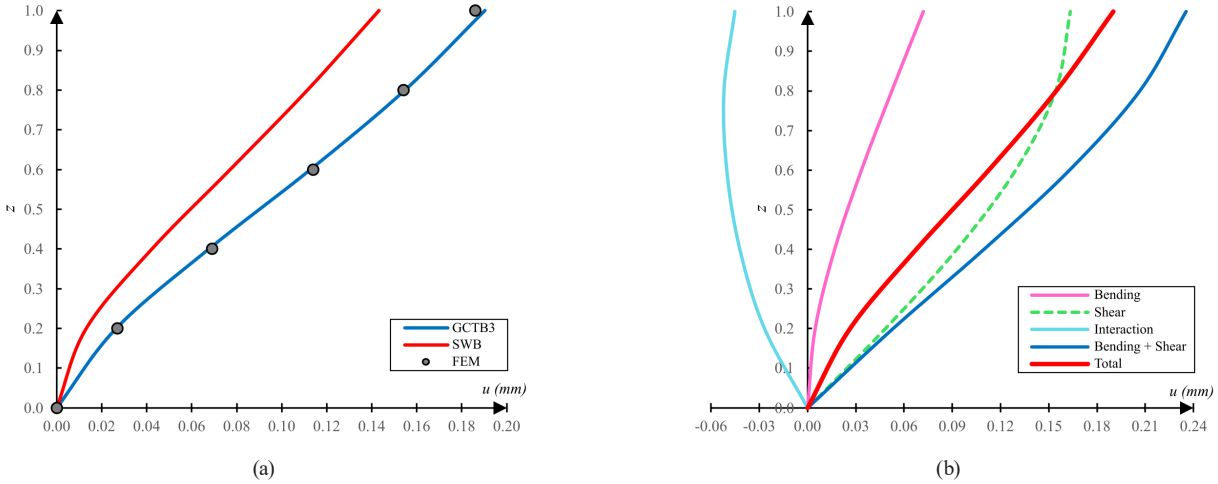

(a) (b)

Fig. 14 Case 1 – Lateral displacement of a 5-story CSW subjected to triangular load: (a) Comparison of lateral displacement results from the GCTB and SWB beam; (b) Decomposition of the GCTB beam displacement into bending, shear, and interaction components

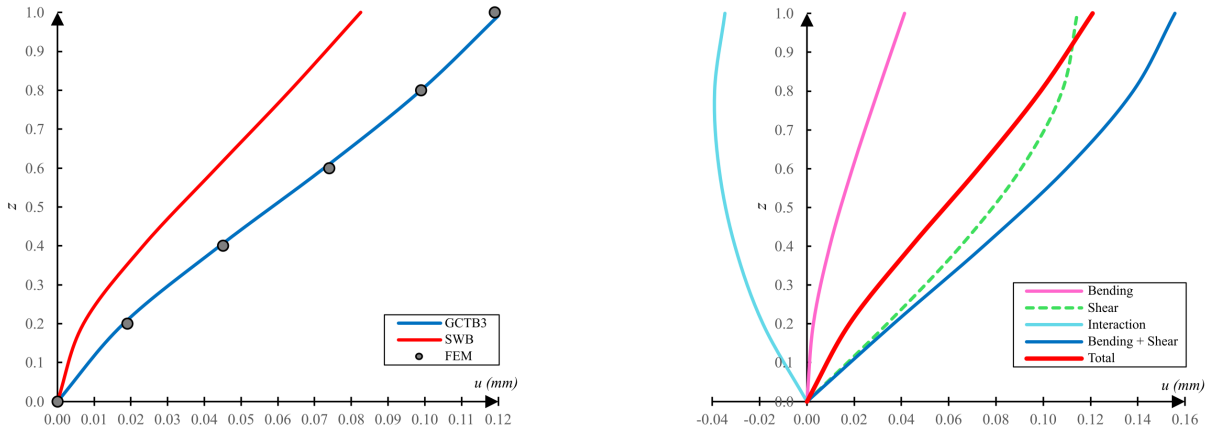

(a) (b)

Fig. 15 Case 2 – Lateral displacement of a 5-story CSW subjected to triangular load: (a) Comparison of lateral displacement results from the GCTB and SWB beam; (b) Decomposition of the GCTB beam displacement into bending, shear, and interaction components

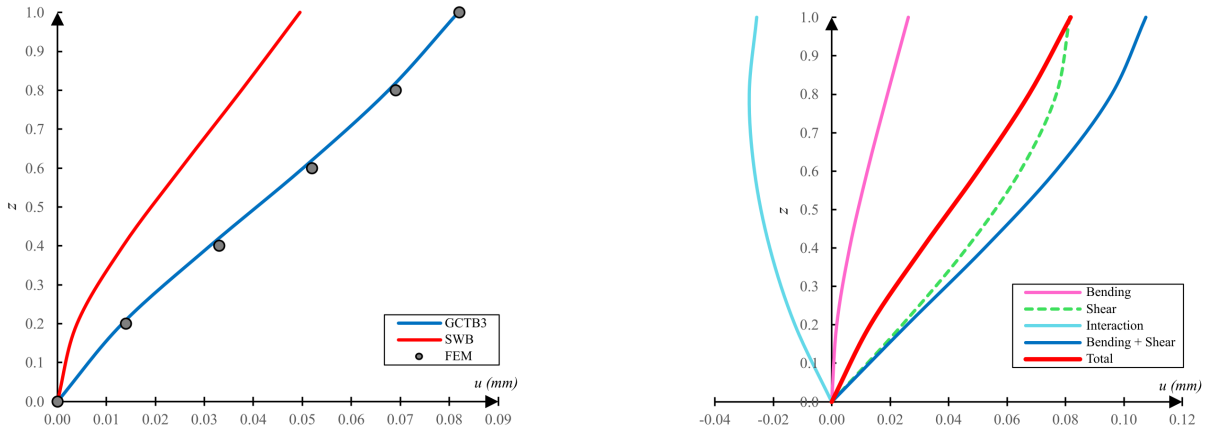

(a) (b)

Fig. 16 Case 3 – Lateral displacement of a 5-story CSW subjected to triangular load: (a) Comparison of lateral displacement results from the GCTB and SWB beam; (b) Decomposition of the GCTB beam displacement into bending, shear, and interaction components

resemble those under uniform loading, differing mainly by a multiplicative factor and a linear term in the interaction component. Consequently, conclusions for uniform loading extend to triangular loading cases. The analytical solutions based on GCTB correspond well with FEM results, validating the formulation for triangular loads.

Under concentrated load applied at the top, the displacement profiles of low-rise CSWs (Figs. 17–19) exhibit a bending-dominated response. This behavior is attributable to the linearity and alignment of shear displacement with the applied load. In this loading scenario, classification by CSW height becomes less meaningful; instead, categorization based on the influence of shear displacement is more appropriate, as shear effects diminish with increasing CSW height. The analytical model closely matches the predictions obtained from the finite element method (FEM), confirming the validity of the proposed solution.

Comparisons with previously published results [30, 31] for low-rise CSWs under uniform and triangular loadings show identical displacement profiles (Fig. 20), corroborating the exactness of the decomposition approach while also demonstrating the excellent accuracy and simplicity of the proposed analytical solutions.

A comprehensive parametric analysis of twelve cases, based on a horizontal bracing system of seven symmetric and identical CSWs [30, 31] under a uniform load ($W = 30$ kN/m), supports the validity of the approach. The classical SWB beam-based results exhibited significant conservative errors (up to −56.04%) and a mean absolute error of +13.24%. In contrast, the proposed solutions reduced the errors to approximately +7.30%, with a mean absolute error of +2.82%, representing a reduction factor of 7.68 (Fig. 21). This asymptotic error behavior supports the safe engineering application of the proposed formulations. Similar validation

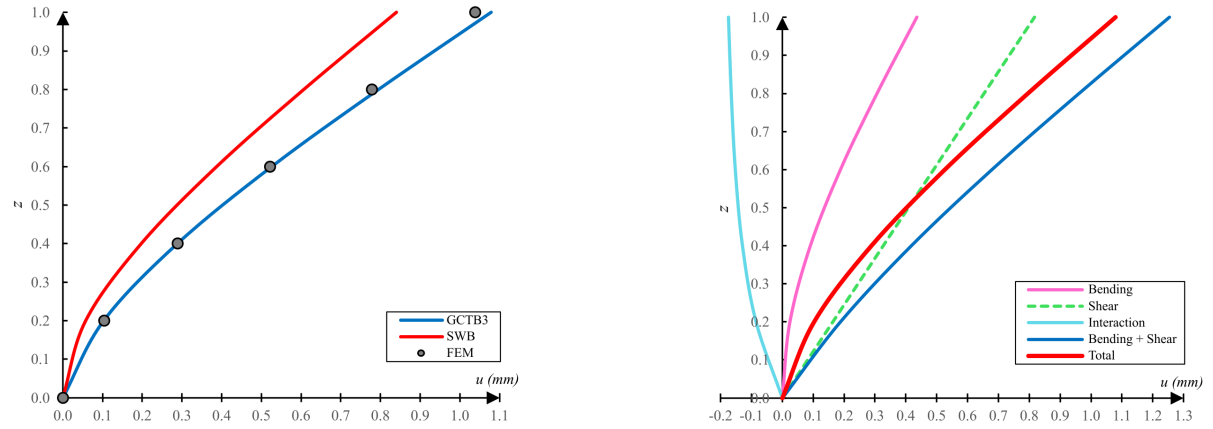

(a) (b)

Fig. 17 Case 1 – Lateral displacement of a 5-story CSW subjected to a concentrated load: (a) Comparison of lateral displacements predicted by the GCTB and SWB beam; (b) Decomposition of the GCTB beam displacement into bending, shear, and interaction components

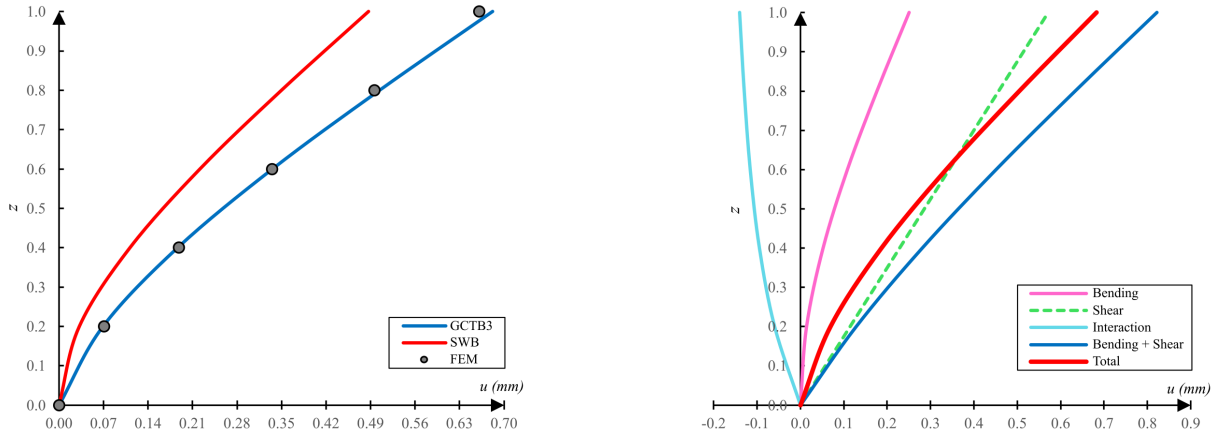

(a) (b)

Fig. 18 Case 2 – Lateral displacement of a 5-story CSW subjected to a concentrated load: (a) Comparison of lateral displacements predicted by the GCTB and SWB beam; (b) Decomposition of the GCTB beam displacement into bending, shear, and interaction components

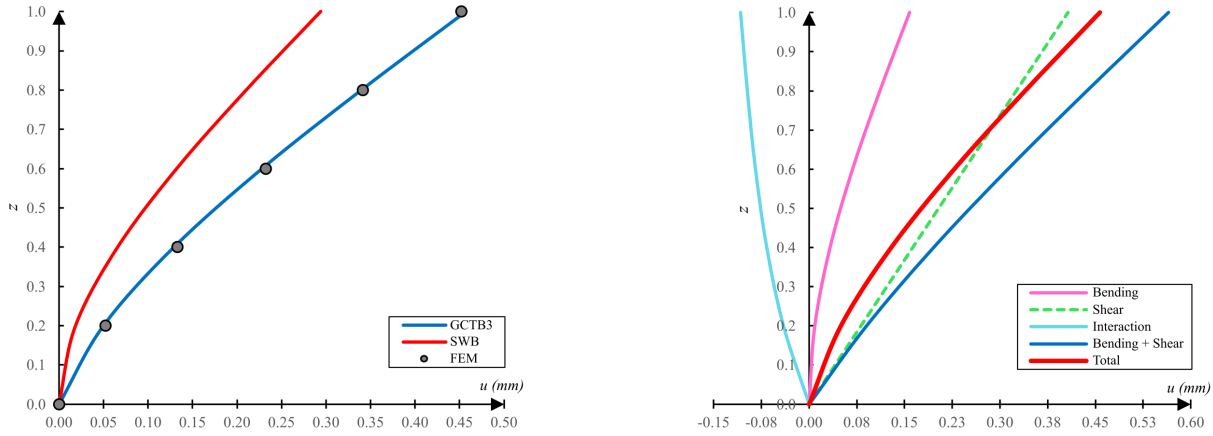

(a) (b)

Fig. 19 Case 3 – Lateral displacement of a 5-story CSW subjected to a concentrated load: (a) Comparison of lateral displacements predicted by the GCTB and SWB beam; (b) Decomposition of the GCTB beam displacement into bending, shear, and interaction components

for triangular and concentrated loading cases demonstrates the superiority of the GCTB beam over the SWB beam. Given the large number of cases considered in the parametric study, these errors were estimated using the equivalent frame approach. However, much smaller errors are expected if the CSW is modeled using plane-stress elements.

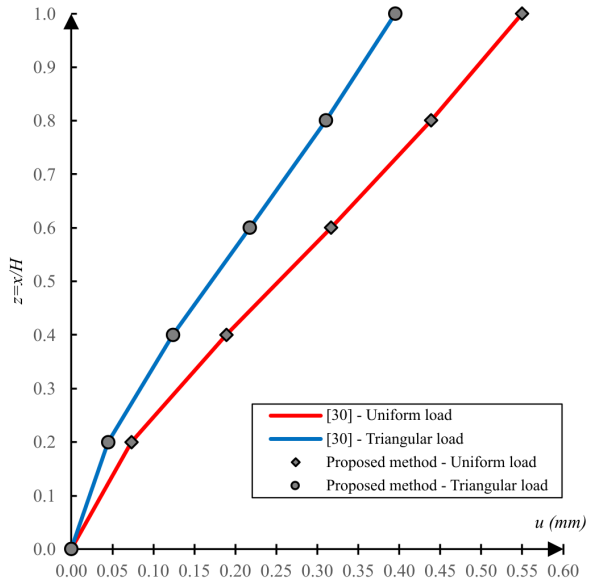

Fig. 20 Comparison of lateral displacement profiles obtained from the proposed analytical solution and those reported in the literature [30, 31]

6 Conclusions

In this study, the GCTB beam was employed to propose exact, simple, and closed-form analytical expressions for estimating the lateral displacement of coupled shear walls (CSWs). The following key conclusions were drawn:

- The GCTB beam extends the classical sandwich beam (SWB beam) formulation by incorporating axial extensibility and local shear deformation of the walls—two deformation mechanisms previously neglected—thus enabling an accurate representation of the four deformation mechanisms of CSWs: global bending, global shear, local bending, and local shear.
- The total lateral displacement can be expressed as the linear combination of three independent subsystems: the EBB beam, the SB beam, and the CTB beam, yielding an exact decomposition.
- Closed-form analytical expressions were proposed for the lateral displacement of CSWs under uniform, triangular, and concentrated loadings, further decomposing the lateral displacement into its three distinctive physical components: bending, shear, and interaction. Bending is governed by the EBB subsystem, shear by the combined SB and CTB subsystems, and interaction exclusively by the CTB subsystem.
- Bending dominates in slender CSWs, whereas shear is significant in low-rise CSWs. Interaction displacement remains nearly constant along the height and becomes more relevant as slenderness decreases.
- For uniform and triangular loadings, variations in equivalent stiffness and height define bending, shear, or interaction dominated regimes. Under top concentrated loading, bending governs the response.
- A static correction factor (η) was introduced to incorporate local shear deformation into the classical solutions. This factor, always greater than unity, is proportional to the square of the total shear stiffness and inversely proportional to the product of the global and local shear stiffnesses. Moreover, it is independent of the CSW height and affects only the lateral displacement component associated with shear and interaction.
- The parametric analysis shows that GCTB beam predictions reduce the maximum unsafe-side error of the SWB beam (−56.04%) to a safe-side error of +7.30%, corresponding to an error reduction factor of 7.67, which is considered acceptable for practical engineering applications.
- The SWB beam is unsuitable when axial extensibility and local shear deformation cannot be neglected, as it produces unsafe displacement estimates. The proposed expressions derived from the GCTB beam retain the simplicity of classical models while significantly improving accuracy.

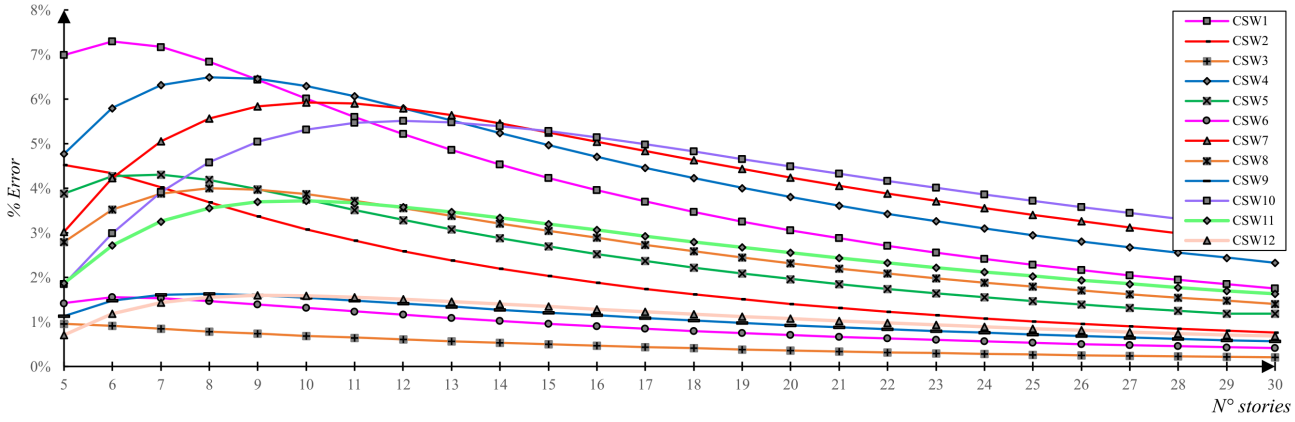

Fig. 21 Error profiles showing the accuracy of lateral displacement predictions obtained from theparametric analysis with the GCTB beam model

The subsystem decomposition strategy confirms that complex static behavior can be addressed in a simple and exact manner through classical, simpler, and decoupled subsystems, thereby enhancing both the physical understanding of the behavior and the derivation of simple analytical expressions. Future research may investigate the dynamic response under seismic excitation by incorporating soil–structure interaction and energy dissipation, may develop approximate solutions to account for nonlinear geometric and material second-order effects, and may experimentally validate the new deformation mechanisms to confirm the accuracy of the model and the role of the recently introduced kinematic fields.

Acknowledgments
This research was made possible through the guidance and support of the Lord Jesus Christ. The author dedicates this contribution to his son, Andrei Joseph, with the hope that it may inspire him to pursue an academic career, exploring and discovering the wonders of science: "*For you, O Lord, are good and forgiving, abounding in steadfast love to all who call upon you. Give ear, O Lord, to my prayer; listen to my plea for grace. In the day of my trouble I call upon you, for you answer me.*" (Psalm 86:5–7).

Conflicts of interest
The author declares no conflicts of interest.

Data availability statement
The data that support the findings of this study are available from the corresponding author upon reasonable request.

References

[1] Computers & Structures "SAP2000, (v24.2.0)", [computer program] Available at: https://www.csiamerica.com/products/sap2000/enhancements/24

[2] Chitty, L. "LXXVIII. On the cantilever composed of a number of parallel beams interconnected by cross bars", The London, Edinburgh, and Dublin Philosophical Magazine and Journal of Science, 38(285), pp. 685–699, 1947. https://doi.org/10.1080/14786444708521646

[3] Chitty, L., Wan, W. Y. "Tall building structures under wind load", In: Proceedings of the Seventh International Congress for Applied Mechanics, London, UK, pp. 254–268, 1948.

[4] Mancini, E., Savassi, W. "Tall building structures unified plane panels behaviour", The Structural Design of Tall Buildings, 8(2), pp. 155–170, 1999. https://doi.org/10.1002/(SICI)1099-1794(199906)8:2%3C155::AID-TAL125%3E3.0.CO;2-6

[5] Mancini, E., Savassi, W. "Three-dimensional association of bending moment and shear force deformable panels", The Structural Design of Tall Buildings, 10(1), pp. 27–42, 2001. https://doi.org/10.1002/tal.166

[6] Franco, C., Chesnais, C., Semblat, J.-F., Giry, C., Desprez, C. "Finite element formulation of a homogenized beam for reticulated structure dynamics", Computers and Structures, 261–262, 106729, 2022. https://doi.org/10.1016/j.compstruc.2021.106729

[7] Bozdogan, K. B. "An approximate method for static and dynamic analyses of symmetric wall-frame buildings", The Structural Design of Tall and Special Buildings, 18(3), pp. 279–290, 2009. https://doi.org/10.1002/tal.409

[8] Bozdogan, K. B., Ozturk, D., Nuhoglu, A. "An approximate method for static and dynamic analyses of multi-bay coupled shear walls", The Structural Design of Tall and Special Buildings, 18(1), pp. 1–12, 2009. https://doi.org/10.1002/tal.390

[9] Laier, J. E. "An improced continuous medium technique for structural frame analysis", The Structural Design of Tall and Special Buildings, 17(1), pp. 25–38, 2008. https://doi.org/10.1002/tal.309

[10] Hegedűs, I., Kollár, L. P. "Buckling of sandwich columns with thick faces subjected to axial loads of arbitrary distribution", Acta Technica Academiae Scientiarum Hungaricae, 97(1–4), pp. 123–131, 1984.

[11] Kollár, L. P. "Buckling analysis of coupled shear walls by the multilayer sandwich model", Acta Technica Academiae Scientiarum Hungaricae, 99(3–4), pp. 317–332, 1986.

[12] Potzta, G., Kollár, L. P. "Analysis of buildings structures by replacement sandwich beams", International Journal of Solids and Structures, 40(3), pp. 535–553, 2003. https://doi.org/10.1016/S0020-7683(02)00622-4

[13] Tarján, G., Kollár, L. P. "Approximate analysis of buildings structres with identical stories subjected to earthquakes", International Journal of Solids and Structures, 41(5–6), pp. 1411–1433, 2004. https://doi.org/10.1016/j.ijsolstr.2003.10.021

[14] Zalka, K. A. "A simple method for the deflection analysis of tall wall-frame building structure under horizontal load", The Structural Design of Tall and Special Buildings, 18(3), pp. 291–311, 2009. https://doi.org/10.1002/tal.410

[15] Zalka, K. "Structural Analysis of Multi-Storey Buildings", CRC Press, 2020. ISBN 978-0-367-35025-3 https://doi.org/10.1201/9780429329371

[16] Zalka, K. A. "A simplified method for calculation of the natural frequencies of wall-frame buildings", Engineering Structures, 23(12), pp. 1544–1555, 2001. https://doi.org/10.1016/S0141-0296(01)00053-0

[17] Zalka, K. A. "Buckling analysis of buildings braced by frameworks, shear walls and cores", The Structural Design of Tall Buildings, 11(3), pp. 197–219, 2002. https://doi.org/10.1002/tal.194

[18] Xu, G., Li, A. "Research on the response of concrete cavity shear wall under lateral load", The Structural Design of Tall and Special Buildings, 28(3), e1577, 2019.
https://doi.org/10.1002/tal.1577

[19] Hu, H.-S., Wang, R.-T., Guo, Z.-X., Shahrooz, B. M. "A generalized method for estimating drifts and drift components of tall buildings under lateral loading", The Structural Design of Tall and Special Buildings, 29(2), e1688, 2020.
https://doi.org/10.1002/tal.1688

[20] Wang, R.-T., Hu, H.-S., Guo, Z.-X. "Analytical study of stiffened multibay planar coupled shear walls", Engineering Structures, 244, 112770, 2021.
https://doi.org/10.1016/j.engstruct.2021.112770

[21] Zhang, L., Liu, T., Chen, Y. "Calculations of additional axial force and coupling ratio for coupled shear walls", Structures, 47, pp. 1531–1547, 2023.
https://doi.org/10.1016/j.istruc.2022.11.126

[22] Tong, G., Lin, C. "Relations between buckling & vibrational characteristics of coupled shear walls", Structures, 31, pp. 1173–1184, 2021.
https://doi.org/10.1016/j.istruc.2021.01.084

[23] Capuani, D., Merli, M., Savoia, M. "An equivalent continuum approach for coupled shear walls", Engineering Structures, 16(1), pp. 63–73, 1994.
https://doi.org/10.1016/0141-0296(94)90105-8

[24] Capuani, D., Savoia, M., Laudiero, F. "Continuum Model for Analysis of Multiply Connected Perforated Cores", Journal of Engineering Mechanics, 120(8), pp. 1641–1660, 1994.
https://doi.org/10.1061/(ASCE)0733-9399(1994)120:8(1641)

[25] Capuani, D., Klein, R., Antes, H., Tralli, A. "Dynamic soil–structure interaction of coupled shear walls by boundary element method", Earthquake Engineering Structural Dynamics, 24(6), pp. 861–879, 1995.
https://doi.org/10.1002/eqe.4290240606

[26] Capuani, D., Merli, M., Savoia, M. "Dynamic analysis of coupled shear wall-frame systems", Journal of Sound and Vibration, 192(4), pp. 867–883, 1996.
https://doi.org/10.1006/jsvi.1996.0222

[27] Capsoni, A., Moghadasi Faridani, H. "Novel continuum models for coupled shear wall analysis", The Structural Design of Tall and Special Buildings, 25(10), pp. 444–467, 2016.
https://doi.org/10.1002/tal.1267

[28] Faridani, H. M., Capsoni, A. "A modified replacement beam for analyzing building structures with damping systems", Structural Engineering and Mechanics, 58(5), pp. 905–929, 2016.
https://doi.org/10.12989/sem.2016.58.5.905

[29] Moghadasi Faridani, H., Capsoni, A. "Analysis of passively-damped coupled shear walls using continuum-based models", Engineering Structures, 148, pp. 739–754, 2017.
https://doi.org/10.1016/j.engstruct.2017.07.007

[30] Pinto, M. C. "Closed-form and numerical solution of the static and dynamic analysis of coupled shear walls by the continuous method and the modified transfer matrix method", Structural Engineering and Mechanics, 86(1), pp. 49–68, 2023.
https://doi.org/10.12989/sem.2023.86.1.049

[31] Pinto-Cruz, M. C. "A general simplified method for static and free vibration analysis of coupled shear walls of a bay", Mechanics Based Design of Structures and Machines, 52(8), pp. 5915–5943, 2024.
https://doi.org/10.1080/15397734.2023.2265466

[32] Pinto-Cruz, M. C. "Analytical solutions for the stability analysis of coupled shear walls: Three-field CTB beam", Mechanics Based Design of Structures and Machines, 53(6), pp. 4502–4541, 2025.
https://doi.org/10.1080/15397734.2025.2451681